Zhao et al. *Light: Science & Applications* (2025)14:227
https://doi.org/10.1038/s41377-025-01899-7

ARTICLE Open Access

All-on-chip reconfigurable generation of scalar and vectorial orbital angular momentum beams

Weike Zhao[1], Xiaolin Yi[1], Jieshan Huang[2], Ruoran Liu[1], Jianwei Wang[2], Yaocheng Shi[1], Yungui Ma[1], Andrew Forbes[1,3]✉ and Daoxin Dai[1]✉

Abstract

Structured light carrying angular momentum, such as spin angular momentum (SAM) and orbital angular momentum (OAM), has been at the core of new science and applications, driving the need for compact on-chip sources. While many static on-chip solutions have been demonstrated, as well as on-chip sources of free-space modes, no architecture that is fully reconfigurable in all angular momentum states and all on-chip has so far been possible. Here we report the first all-on-chip structured light generator for the creation of both scalar and vectorial angular momentum beams, facilitated through a silicon-on-insulator (SOI) chip with a silica mode multiplexer (silica chip). We selectively stimulate six linearly-polarized (LP) modes of the silica multimode bus waveguide, precisely controlling the modal powers and phases with the SOI chip. This allows us to tailor arbitrary superpositions of the mode set thus synthesizing common cylindrical vector vortex beams as well as OAM beams of controlled spin and topological charge. Our compact structured light generator exhibits high switching speed and operates across the telecom band, paving the way for applications such as optical communication and integrated quantum technologies.

Introduction

In recent decades, structured light has captured a great deal of research interest and found a variety of applications[1–4], including spin angular momentum (SAM) beams[5,6], cylindrical vector (CV) beams[7,8], orbital angular momentum (OAM) beams[9,10], and total angular momentum (TAM) beams[11,12], which have special spatial distributions of intensity, phase or polarization. Among them, SAM beams are associated with circular polarization and carry SAM of $S=\sigma\hbar$ ($\sigma=\pm1$) per photon, while CV beams feature a circular symmetry polarization distribution and are undetermined at the beam center where there is a polarization singularity. CV beams have shown great potential in various applications, such as plasmonic nanofocusing[13,14], particle manipulation[15], and high-resolution optical microscopy[16], due to their unique focusing property. In contrast, OAM beams have a helical phase front characterized by Hilbert factor $\exp(il\theta)$, where l is the topological charge value and θ is the azimuthal angle[17], resulting in a phase singularity at the beam center and an OAM of $l\hbar$ per photon. The unique phase/intensity distribution of OAM beams makes them very useful for widespread applications, including mode-division multiplexing[18,19], optical micro-manipulation[20–22], and optical measurement[23] to name but a few.

The myriad of applications has fueled the generation of structured light, with the bulk optick toolkit now comprising spatial light modulators[24,25], fiber-based devices[7–9,26–30], spiral phase plates[31] and directly from lasers[32,33]. On-chip structured light generators come with the advantages of compactness, robustness, and versatility, and have attracted significant attention of late. A variety of silicon-on-insulator (SOI) photonic structures have been demonstrated for generating structured light[34–43]. On-chip metamaterials or metasurfaces imply a helical wavefront on the launched light by using a set of meta-atoms that offer a phase modulation of 0-2π with the principle of electric dipole resonance and generalized laws of reflection/refraction, and have been widely used to

Correspondence: Andrew Forbes (Andrew.Forbes@wits.ac.za) or Daoxin Dai (dxdai@zju.edu.cn)
[1]State Key Laboratory for Extreme Photonics and Instrumentation, College of Optical Science and Engineering, Zhejiang University, Hangzhou 310058, China
[2]State Key Laboratory for Mesoscopic Physics, School of Physics, Peking University, Beijing 100871, China
Full list of author information is available at the end of the article
These authors contributed equally: Weike Zhao, Xiaolin Yi.

© The Author(s) 2025
Open Access This article is licensed under a Creative Commons Attribution 4.0 International License, which permits use, sharing, adaptation, distribution and reproduction in any medium or format, as long as you give appropriate credit to the original author(s) and the source, provide a link to the Creative Commons licence, and indicate if changes were made. The images or other third party material in this article are included in the article's Creative Commons licence, unless indicated otherwise in a credit line to the material. If material is not included in the article's Creative Commons licence and your intended use is not permitted by statutory regulation or exceeds the permitted use, you will need to obtain permission directly from the copyright holder. To view a copy of this licence, visit http://creativecommons.org/licenses/by/4.0/.

emit the OAM beams. By further utilizing the spin-orbit conversion, metamaterial also performs controllable transformation between SAM and OAM beams[39,40]. Alternatively, holographic gratings, which are compact and efficient, can couple an in-plane guided-mode to a free-space OAM mode by introducing subwavelength surface structures[41,42]. In addition, dielectric or plasmonic cavities with strong mode coupling have also been developed for on-chip OAM beam generation by using angular gratings to achieve free-space OAM beams with well-controlled topological charges from in degenerate whispering gallery modes (WGM). The different order cavity-modes at discrete resonance wavelengths map to the OAM beams carrying different topological charge values l[43], and the emitting OAM order can be tuned by using an electrical heater[38] or utilizing the strong mutual interaction of the SAM and OAM[34–37]. It should be mentioned that the aforementioned schemes are all based on the optical diffraction mechanism, and their conversion efficiency is limited to <~25% due to the downward emission to the substrate[42]. A potential solution to improve emission efficiency is coating a reflection layer on the substrate[44] or adopting unidirectional radiation grating[45]. Furthermore, the large divergence angle of diffraction structures also makes them difficult to be coupled to OAM fibers, which thus hinders their further applications.

More recently, photonic integrated circuits (PICs) have been used to create scalar structured light modes[46,47], a nascent direction that holds exciting future promise for structured light generators. In recent advances, the light was injected into the device, amplitude and phase modulated on-chip through a PIC, and then tailored in free-space by interference[47] or by using a fixed metasurface[46], producing scalar free-space modes. To realize a compact and reconfigurable approach that extends to arbitrary angular momentum beams that are controlled all on-chip (without free-space coupling) would require engineering spatial modes on the basis of on-chip waveguides or fibers and non-separably combining them with polarization, in principle allowing all-on-chip reconfigurable angular momentum creation from scalar to vectorial states of SAM and OAM light. While this is highly desirable for fully integrated functionality, it has yet to be realized[48].

In this paper, we advance the nascent field of PICs as beam creators by demonstrating an all-on-chip reconfigurable structured light generator that produces on-demand angular momentum beams, from scalar vortex beams to vector vortex beams, all as natural fiber modes. We achieve this by using the natural modes of the silica waveguide as our basis set, controlled by six independent outputs of an SOI chip from three ports (each with two orthogonal polarizations), each reconfigurable in modal power and phase. We demonstrate this for a controlled spin and topological charge of OAM modes of order 1, as well as their vectorial combinations, including the well-known cylindrical vector vortex beams, e.g., radially and azimuthally polarised light. Our PIC architecture merges an SOI chip and a silica mode multiplexer (silica chip) for a compact device, while the all-on-chip configuration is ensured by the fiber coupled input and the subsequent on-chip excitation of scalar and vectorial OAM inside the silica multimode bus waveguide (MBW), circumventing the deleterious free-space to chip input/output coupling. Our convenient all-on-chip generation of structured light enjoys fast switching speed, a broad working bandwidth, high conversion efficiency, easy fiber-coupling (input and output), and can be extended in the future to higher OAM values and arbitrary total angular momentum by simply scaling the SOI chip output ports and MBW size without any fundamental changes to the concept or geometry.

Results

Concept and Implementation

Our concept involves the exploitation of the SOI chip for light with controlled amplitude and phase at several output ports, using this to control the superposition of modes in a silica waveguide/fiber by edge coupling, and then finally dynamically adjusting the SOI chip to produce any desired OAM mode directly on a chip within the silica waveguide/fiber by appropriate superposition of the underlying modes. To unpack this by way of example, note that both few-mode fibers (FMFs) and square silica waveguides with appropriate cross-section parameters can support the well-known Linearly Polarised (LP) mode set, with six such LP modes (i.e., $LP_{01\text{-}x}$, $LP_{01\text{-}y}$, $LP_{11a\text{-}x}$, $LP_{11a\text{-}y}$, $LP_{11b\text{-}x}$, and $LP_{11b\text{-}y}$) shown in Fig. 1a. From these, it is possible to construct, by appropriate superpositions, both scalar and vectorial OAM modes of topological order 1, following[3]

$$\mathrm{SAM}_{\pm 1} = (\mathrm{LP}_{01-x} \mp i \cdot \mathrm{LP}_{01-y})/\sqrt{2} \tag{1a}$$

$$\mathrm{RPB} = (\mathrm{LP}_{11a-x} - \mathrm{LP}_{11b-y})/\sqrt{2}\ \mathrm{or}\ (\mathrm{LP}_{11a-x} + i \cdot \mathrm{LP}_{11b-y})/\sqrt{2} \tag{1b}$$

$$\mathrm{APB} = (\mathrm{LP}_{11a-y} - \mathrm{LP}_{11b-x})/\sqrt{2}\ \mathrm{or}\ (\mathrm{LP}_{11a-y} + i \cdot \mathrm{LP}_{11b-x})/\sqrt{2} \tag{1c}$$

$$\mathrm{OAM}_{\pm 1-x} = (\mathrm{LP}_{11a-x} \pm i \cdot \mathrm{LP}_{11b-x})/\sqrt{2} \tag{1d}$$

$$\mathrm{OAM}_{\pm 1-y} = (\mathrm{LP}_{11a-y} \pm i \cdot \mathrm{LP}_{11b-y})/\sqrt{2} \tag{1e}$$

Here the subscript numbers are radial and azimuthal mode orders, a/b is the horizontal/vertical mode azimuth,

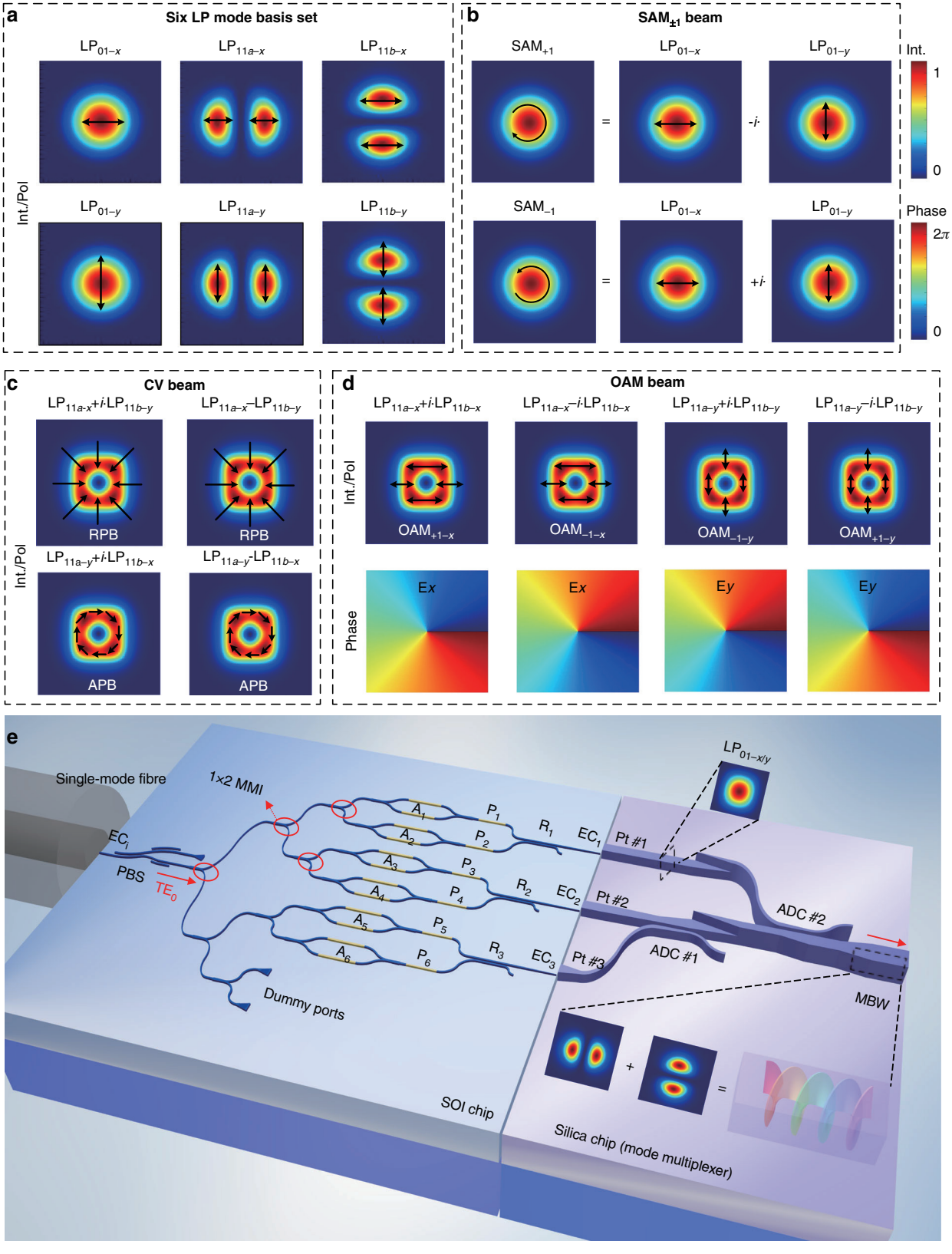

Fig. 1 (See legend on next page.)

(see figure on previous page)
Fig. 1 All-on-chip structured light generator. a Six LP mode basis sets at a few-mode fiber or a square silica waveguide, i.e., $LP_{01\text{-}x}$, $LP_{01\text{-}y}$, $LP_{11a\text{-}x}$, $LP_{11a\text{-}y}$, $LP_{11b\text{-}x}$, and $LP_{11b\text{-}y}$ modes. **b** Top panel: the SAM_{+1} beam (right-handed circular polarization) is synthesized by the $LP_{01\text{-}x}$ and $LP_{01\text{-}y}$ modes with a phase difference of π/2; bottom panel: the SAM_{-1} beam (left-handed circular polarization) is synthesized by the $LP_{01\text{-}x}$ and $LP_{01\text{-}y}$ modes with a phase difference of -π/2. **c** The intensity/polarization patterns of the CV beams containing RPB and APB, which both have donut intensity patterns, but are distinguished with radial and azimuthal polarization, respectively. **d** The intensity/polarization patterns and phase structures of the $OAM_{\pm1\text{-}x}$ and $OAM_{\pm1\text{-}y}$ beams. **e** Schematic configuration of the proposed all-on-chip structured light generator incorporating an SOI chip and a silica chip. Upper inset: the $LP_{01\text{-}x/y}$ mode in a silica single mode waveguide; Bottom inset: the $OAM_{\pm1}$ beam is synthesized as an example by using the LP_{11a} and LP_{11b} modes in a silica multimode bus waveguide (MBW). Operating principle: the light emitted by the fiber to the SOI chip is polarized with a polarization beam splitter (PBS) and then split into six TE_0 modes with a series of 1×2 multimode-interference (MMI) 3-dB couplers. These six TE_0 modes respectively pass through a variable optical attenuator (VOA) and a phase shifter (PS), and then are combined into three pairs of TE_0/TM_0 modes by three polarization splitter-rotators (PSR, R_1-R_3). These three pairs of TE_0/TM_0 mode are coupled to the $LP_{01\text{-}x}$/ $LP_{01\text{-}y}$ modes of three silica waveguide ports (Pt #1, Pt #2, and Pt #3) by three edge couplers (ECs, EC_1-EC_3). Finally, these three pairs of $LP_{01\text{-}x}/LP_{01\text{-}y}$ modes stimulate the six LP mode basis sets of the MBW through a silica mode multiplexer (containing two adiabatic directional couplers, ADC #1 and ADC #2). One can selectively synthesize the $SAM_{\pm1}$, $OAM_{\pm1\text{-}x}/OAM_{\pm1\text{-}y}$ beams, as well as the CV beams by controlling the powers and phases of these six LP modes with the six VOAs (A_1-A_6) and PSs (P_1-P_6)

and-x/-y is the horizontal/vertical polarization. Higher numbers of LP modes would naturally allow higher-order OAM modes to be engineered. Continuing with our example, we see that the desired modes can be synthesized by selectively combining these six LP modes with specific modal powers and phases, which we achieve with the PIC. For instance, the $SAM_{\pm1}$ beam can be synthesized by combining the $LP_{01\text{-}x}$ and $LP_{01\text{-}y}$ modes with a phase difference of π/2 (for right-handed circular polarization) or -π/2 (for left-handed circular polarization) according to Eq. (1a), as shown in Fig. 1b. Note that CV beams contain the radially polarized beam (RPB) and the azimuthally polarized beam (APB), while the RPB and APB can be synthesized with the LP_{11a} and LP_{11b} modes with different polarizations by following Eqs. (1b) and (1c), respectively. The intensity/polarization distributions of the RPB and APB are clearly shown in Fig. 1c, which both have donut intensity patterns, but are distinguished with radial and azimuthal polarization, respectively. Furthermore, as given in Eqs. (1d) and (1e), the *x*- and *y*-polarized $OAM_{\pm1}$ beams (i.e., $OAM_{\pm1\text{-}x}$ and $OAM_{\pm1\text{-}y}$) can be synthesized by combining the LP_{11a} and LP_{11b} modes with the same polarization. Figure 1d shows the doughnut-shaped field distributions of the $OAM_{\pm1\text{-}x}$ and $OAM_{\pm1\text{-}y}$ beams as well as the spiral phase structures for their E_x and E_y components.

As a summary, the aforementioned structured light can intuitively be synthesized by exciting two specific power-, polarization- and phased-controlled LP modes. Even though LP modes are well supported in low-index-contrast optical waveguides (such as silica waveguides or fibers), the manipulation of the polarization state and the phase shifting becomes very inconvenient due to the low polarization-selectivity and low thermal-tuning efficiency. In contrast, when using silicon waveguides (which have a high index contrast), it becomes very flexible to manipulate the polarization states, the power ratios, and the phase shifts of the guided modes. As a consequence, here we propose a new PIC structured light generator by incorporating an SOI chip and a silica chip, as shown in Fig. 1e. In particular, the SOI chip is used for manipulating the polarization states, the power ratios and the phase-shiftings of the guided light, so that three pairs of TE_0/TM_0 modes are generated with flexibly tunable power ratios and phase shifts. The silica chip is used to receive these three pairs of TE_0/TM_0 modes from the SOI chip and then multiplex them to the six quasi LP modes basis sets (i.e., $LP_{01\text{-}x}$, $LP_{01\text{-}y}$, $LP_{11a\text{-}x}$, $LP_{11a\text{-}y}$, $LP_{11b\text{-}x}$, $LP_{11b\text{-}y}$) supported in a silica MBW. With such a configuration, the power ratios and phase shifts of these six LP modes can be controlled freely by tuning the heaters on the SOI chip, and thus the $SAM_{\pm1}$, $OAM_{\pm1\text{-}x}$, and $OAM_{\pm1\text{-}y}$ and RPB/APB beams can selectively be synthesized.

As shown in Fig. 1e, light from a single-mode fiber is coupled to the input port of the SOI chip with the assistance of silicon edge couplers (EC_i) and is polarized to be the TE_0 mode by using a polarization beam splitter (PBS)[49]. The TE_0 mode is then split by using a 1×8 power splitter based on 1×2 multimode-inteference (MMI) 3-dB couplers in cascade. Note that there are two dummy ports used for splitting ratio and insertion loss measurement. For these six TE_0 modes, there are six variable optical attenuators (VOAs; A_1, A_2, …, A_6) to manipulate the power ratios and six phase shifters (PSs; P_1, P_2, …, P_6) to manipulate the phase shifts[50], respectively. These six TE_0 modes with the target power ratios and phase shifts are then recombined to be three TE_0/TM_0 mode-pairs by using three polarization splitter-rotators (PSRs; R_1, R_2, R_3)[51,52] and output finally from Ports (Pt) #1, #2, and #3, respectively (see Methods). The SOI chip is butt coupled to the silica chip with three ECs (EC_1, EC_2, EC_3), in which way the three pairs of TE_0/TM_0 modes in the three silicon waveguides are coupled respectively to the $LP_{01\text{-}x}/LP_{01\text{-}y}$ modes of three silica single mode waveguides. Finally, these $LP_{01\text{-}x}/LP_{01\text{-}y}$ modes are converted and multiplexed to the six LP modes basis sets (i.e., $LP_{01\text{-}x}$, $LP_{01\text{-}y}$, $LP_{11a\text{-}x}$, $LP_{11a\text{-}y}$, $LP_{11b\text{-}x}$, $LP_{11b\text{-}y}$) supported in the MBW, by using a

polarization-insensitive silica mode multiplexer, which consists of two adiabatic directional couplers (ADCs; ADC #1, ADC #2) in cascade. In detail, the LP_{01} mode launched from Port #1 couples to the LP_{11a} mode of the MBW via ADC #2, while the LP_{01} mode launched from Port #3 couples to the LP_{11a} mode of the MBW via ADC #1 and then is rotated to the LP_{11b} mode with a mode rotator based on a dual-layer silica waveguide. Here the LP_{01} mode launched from Port #2 transmits through these two ADCs directly (see Methods). The transmission of the whole PIC structured light generator can be depicted by the transmission matrix method (Supplementary Note 1). Note that while we have outlined this concept based on the implementation of our silica MBW supporting just six modes, it can be generalized to an arbitrary mode number for both higher OAM orders and TAM control.

Fabrication and measurement results

The SOI and silica chips were fabricated separately with their own regular processes (Supplementary Note 2). The PBSs and PSRs fabricated on the SOI chip all have a low loss of <1 dB and crosstalk <-15 dB for both TE_0 and TM_0 mode channels (Supplementary Note 3). The input fiber array, SOI chip, silica chip and FMF were butt-coupled, as shown in Fig. 2a. Here an ultra-high-NA single mode fiber (HSMF) with a numerical aperture of 0.41 and a core diameter of ~2.4 μm was used for the butt coupling with the SOI chip through an EC, enabling a relatively low coupling loss of ~2 dB for the TE_0 mode in the wavelength range of 1520–1600 nm. The coupling loss between the silicon waveguide and the $4 \times 4\ \mu m^2$ single mode silica waveguide with the help of the same EC is 0.4/1.5 dB for the TE_0/TM_0 modes (Supplementary Note 3). The silica mode multiplexer has a low on-chip loss of <0.8 dB and low inter-mode crosstalk of <-14.2 dB for all three modes in the broad wavelength range of 1530–1620 nm[53]. The SOI chip was wire-bonded onto a printed circuit board (PCB) for electrical control. Figure 2b shows the enlarged views of the SOI and silica chips, and the silica waveguide is labeled with a dotted line. The scanning electron microscope (SEM) images of the PBS, MMI coupler, PSR, and silica waveguide are shown in Fig. 2c–f, respectively.

Generation of the six LP-mode basis sets

A multichannel voltage source (MVS) was used to power the six VOAs and six PSs, so that the power ratios and the phase shifts of these six TE_0/TM_0 channels can be controlled (Supplementary Note 4). Figure 3a, b gives the measurement results for the VOAs, showing an excess loss of <0.6 dB and a maximum extinction ratio of ~26 dB at the wavelength of ~1580 nm. The thermal tuning of the VOAs and PSs works with a rise time T_r of 11.6 μs and a falling time of T_f of 7.1 μs, enabling fast generation of structured light beams. This performance benchmark is

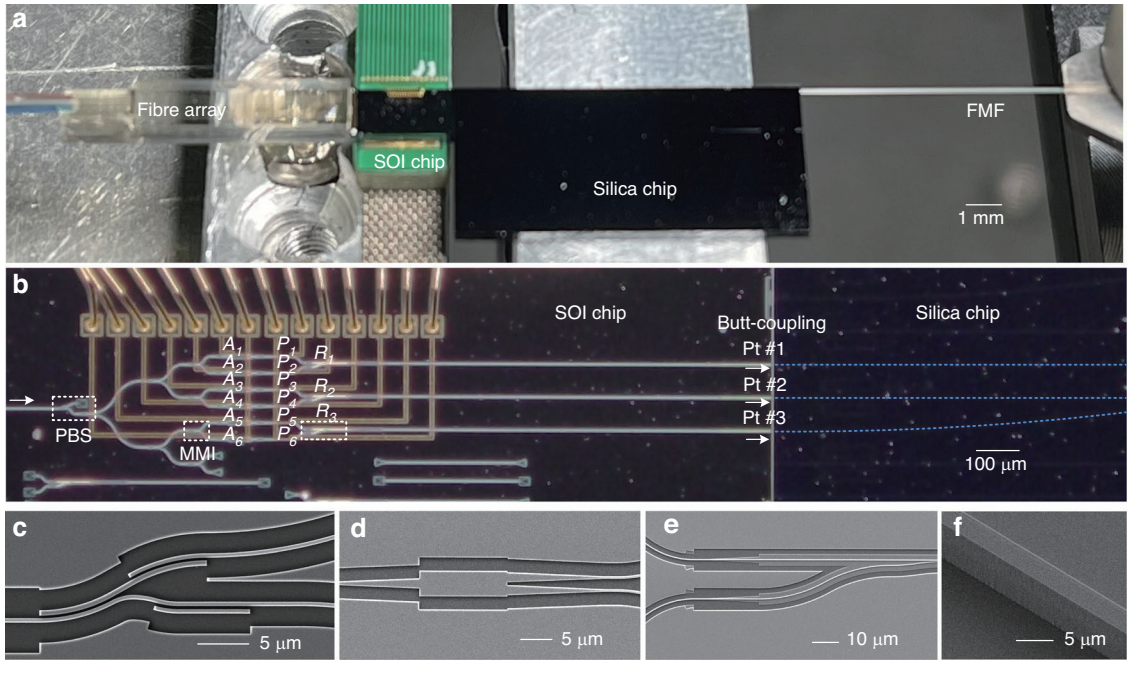

Fig. 2 Images of the fabricated device. a The butt-coupled input fiber array, SOI chip, silica chip and FMF. **b** The enlarged view of the butt-coupled SOI chip and silica chip, where the PBS, MMI, VOAs (A_1-A_6), PSs (P_1-P_6), PSRs (R_1-R_3), three ports (Pt #1-#3) are labeled. Scanning electron microscope (SEM) images were given for the (**c**) PBS, (**d**) MMI coupler, (**e**) PSR, and (**f**) silica waveguide

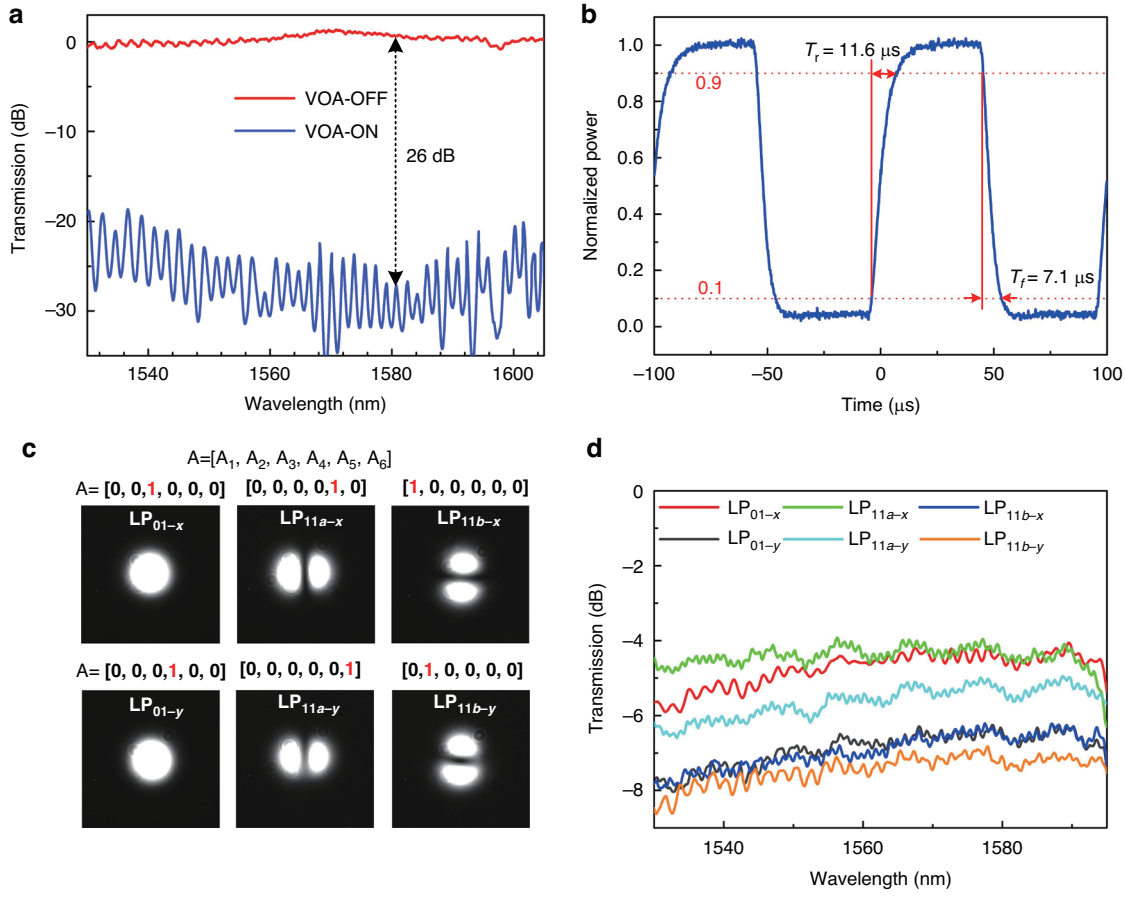

Fig. 3 Characterization of VOAs and the excitation of the six LP mode basis sets. a The measured on/off transmissions of the testing VOA fabricated on the same SOI chip, showed a maximum extinction ratio of ~ 26 dB at 1580 nm. **b** The measured temporal response of the VOA, exhibits a rise time T_r of 11.6 μs and a falling time T_f of 7.1 μs. **c** Any one of six LP-modes excited individually in the MBW by controlling the VOAs to achieve the target amplitude matrix A = [A_1, A_2, A_3, A_4, A_5, A_6] as desired. **d** The measured transmissions from the input fiber to the output FMF when any one of these six LP modes is excited individually, show an excess loss of 4-8 dB for all six modes in a broad wavelength range of 1530-1595 nm

comparable to state-of-the-art implementations utilizing optical antenna arrays[36] and angular grating-integrated microring resonators[47], which similarly employ thermo-optic modulation for dynamic OAM topological charge control. The response time of the generator can be further reduced to nanosecond lever by utilizing the carrier dispersion effect[47] or electro-optic effect[54]. The amplitude matrix of six LP mode basis sets is given as $\mathbf{A} = [A_1, A_2, A_3, A_4, A_5, A_6]$, where A_m is the amplitude for the m-th mode-channel, and one has $A_m = 1$ or 0 by unheating or heating the m-th VOA (VOA_m). As a result, appropriately controlling the VOAs enables to individually excite any one of the $LP_{01\text{-}x}$, $LP_{01\text{-}y}$, $LP_{11a\text{-}x}$, $LP_{11a\text{-}y}$, $LP_{11b\text{-}x}$, and $LP_{11b\text{-}y}$ modes in the MBW, as shown in Fig. 3c. A pair of silica mode multiplexers connected back to back are fabricated on the same silica chip, and the crosstalk matrix of six LP modes was obtained by measuring their port-to-port transmission. The results concluded in Table 1, show that the mode pairs have an on-chip insertion loss of less than 3.2 dB and mode crosstalk of less than 14.3 dB for all six modes at 1550 nm wavelength[53]. It can be seen that all six LP modes are generated successfully with the desired mode profiles, and the perfect azimuth orthogonality of the LP_{11a} and LP_{11b} modes verifies that the fabricated silica chip performs well.

Table 1 The crosstalk matrix of the six LP modes (dB)

	$LP_{01\text{-}x}$	$LP_{01\text{-}y}$	$LP_{11a\text{-}x}$	$LP_{11a\text{-}y}$	$LP_{11b\text{-}x}$	$LP_{11b\text{-}y}$
$LP_{01\text{-}x}$	−2.53	−32.73	−27.24	−35.35	−22.64	−24.21
$LP_{01\text{-}y}$	−24.12	−1.75	−26.41	−31.22	−20.02	−27.15
$LP_{11a\text{-}x}$	−31.24	−23.01	−2.19	−29.9	−16.45	−19.42
$LP_{11a\text{-}y}$	−20.32	−18.46	−28.49	−1.81	−19.88	−23.02
$LP_{11b\text{-}x}$	−22.05	−23.06	−18.05	−19.16	−3.22	−29.92
$LP_{11b\text{-}y}$	−20.57	−23.36	−22.89	−30.97	−32.69	−2.29

Figure 3d shows the measured transmissions from the input fiber to the output FMF when any one of these six LP modes is excited individually. It can be seen that the SOI and silica chips for the present structured light generator work well with a low excess loss of about 4–8 dB in a broad wavelength range of 1530–1595 nm. Here the excess loss contains the total on-chip losses of about 2 dB, the coupling loss of 0.4/1.5 dB between the silicon and silica chips for x-/y- polarization, and the coupling loss of ~2–4 dB between the silica chip and the few-mode fiber. It should be noted that the majority of the loss stems from the coupling losses between chips and between the chip and the fiber, with the coupling loss between the silica chip and the few-mode fiber being particularly significant. The overall efficiency, defined as the energy in each output mode at the output of the silica chip (without the coupling loss between silica chip and few-mode fiber) over the initial input energy of the source injecting the silicon chip (containing coupling loss between single mode fiber and silicon chip), is estimated to 4.9%, 3.1%, 5.5%, 2.5% and 2.6% for $LP_{01\text{-}x}$, $LP_{01\text{-}y}$, $LP_{11a\text{-}x}$, $LP_{11a\text{-}y}$, $LP_{11b\text{-}x}$, and $LP_{11b\text{-}y}$ modes, respectively. There is potential to further reduce the excess loss through the optimization of the chip architecture and the improvement of the fabrication process.

Synthesis of SAM

For the generation of the $SAM_{\pm1}$ beam, the matrix **A** was set to [0, 0, 1, 1, 0, 0] so that only the $LP_{01\text{-}x}$ and $LP_{01\text{-}y}$ modes in the MBW were excited. The modal powers of these two LP modes were balanced by tuning VOA #3 and #4, while their phase difference was tuned to be π/2 or -π/2 according to Eq. (1a) by adjusting the bias voltages V_{P3} and V_{P4} applied to the phase shifters P_3 and P_4. The generated $SAM_{\pm1}$ beam was characterized by using a common quarter-wave plate (QWP) rotation method (Supplementary Note 4), as shown in Fig. 4a. Here the phase difference becomes π/2 and -π/2 when $V_{P3} = 1.95$ V and 3.5 V, respectively. When $V_{P3} = 1.95$ V, the mode intensity remained unchanged as the polarizer was rotated with different orientation angles of 0°, 45°, 90°, and 135° (see the black arrows) if no QWP was inserted. In contrast, when a QWP with a horizontal fast axis was placed in front of the polarizer, one observed constructive and destructive interference when the polarizer was 45°- and 135°-orientated, respectively, as shown in the middle panel of Fig. 4a, indicating that the generated beam carries SAM_{+1} as expected. When further increasing V_{P3} to 3.5 V, constructive and destructive interference respectively happens when the polarizer is 135°- and 45°-orientated, as shown in the bottom panel of Fig. 4a, indicating the SAM_{-1} beam is generated as desired. Based on the transmittance labeled in Fig. 4a, the purity of the $SAM_{\pm1}$ beams is deduced to be larger than 0.989. Note that the output beam's polarization state can traverse the Poincaré sphere by appropriately setting A_3, A_4 and $V_{P3/4}$.

Synthesis of CV beams

When matrix **A** is set to be [0, 1, 0, 0, 1, 0], the $LP_{11a\text{-}x}$ and $LP_{11b\text{-}y}$ modes in the MBW are excited simultaneously, and their phase difference can be tuned to 0 or -π/2, in which case the RPB beam is generated according to Eq. (1b). As shown by the top panel in Fig. 4b, the synthesized mode field has a donut-shaped intensity when $V_{P2} = 1.5$ V. When a polarizer with rotated orientation angles is inserted before the CCD camera, a series of LP_{11} mode fields with different azimuth are achieved (red arrow) and the LP_{11} mode's azimuth is perfectly consistent with the polarizer orientation angles, verifying that the generated CV beam is RPB. In contrast, matrix **A** should be set as [1, 0, 0, 0, 0, 1] to synthesize the APB according to Eq. (1c), in which way the $LP_{11a\text{-}y}$ and $LP_{11b\text{-}x}$ modes are excited simultaneously. A donut intensity pattern appears when $V_{P1} = 1.7$ V, as shown in the bottom panel of Fig. 4b, while the azimuth of the LP_{11} mode is perpendicular to the polarizer's transmission axis, as expected. The nonideal intensity pattern of the CV beam may be due to the unfavorable orientation of the modal basis, and one can optimize the design of the silica mode multiplexer to achieve a better LP mode basis set. Moreover, the unbalanced power ratio and phase difference of the two basis modals can also induce this result. To address this problem, one can optimize the architecture of the generator, thus decreasing and balancing the insertion loss of each channel on the one hand. On the one hand, more attention should be paid to the thermal management of the silicon chip, thus controlling the power and phase of these mode channels accurately. Nevertheless, the vector quality factor can be extracted using Concurrence as a measure[55], determining the nonseparability of the field. With this approach, we find purity values of 0.9788 and 0.9986 for the two vectorial modes as labeled in Fig. 4b, respectively.

Synthesis of OAM beams

To generate $OAM_{\pm1}$ beams, the LP_{11a} and LP_{11b} modes with the same polarization should be stimulated according to Eqs. (1d) and (1e). To verify the phase information of the generated OAM beams, an interference measurement method was used (Supplementary Note 4). For the synthesis of $OAM_{+1\text{-}x}$, the $LP_{11a\text{-}x}$ and $LP_{11b\text{-}x}$ modes should be excited simultaneously and accordingly matrix **A** is set as [1, 0, 0, 0, 1, 0]. As shown in the top panel of Fig. 4c, one observes a donut-shaped intensity pattern and a clockwise helical coaxial interference pattern when setting $V_{P1} = 2.0$ V for achieving the desired π/2 phase difference between the $LP_{11a\text{-}x}$ and $LP_{11b\text{-}x}$ modes, which indicates that the $OAM_{-1\text{-}x}$ beam is synthesized

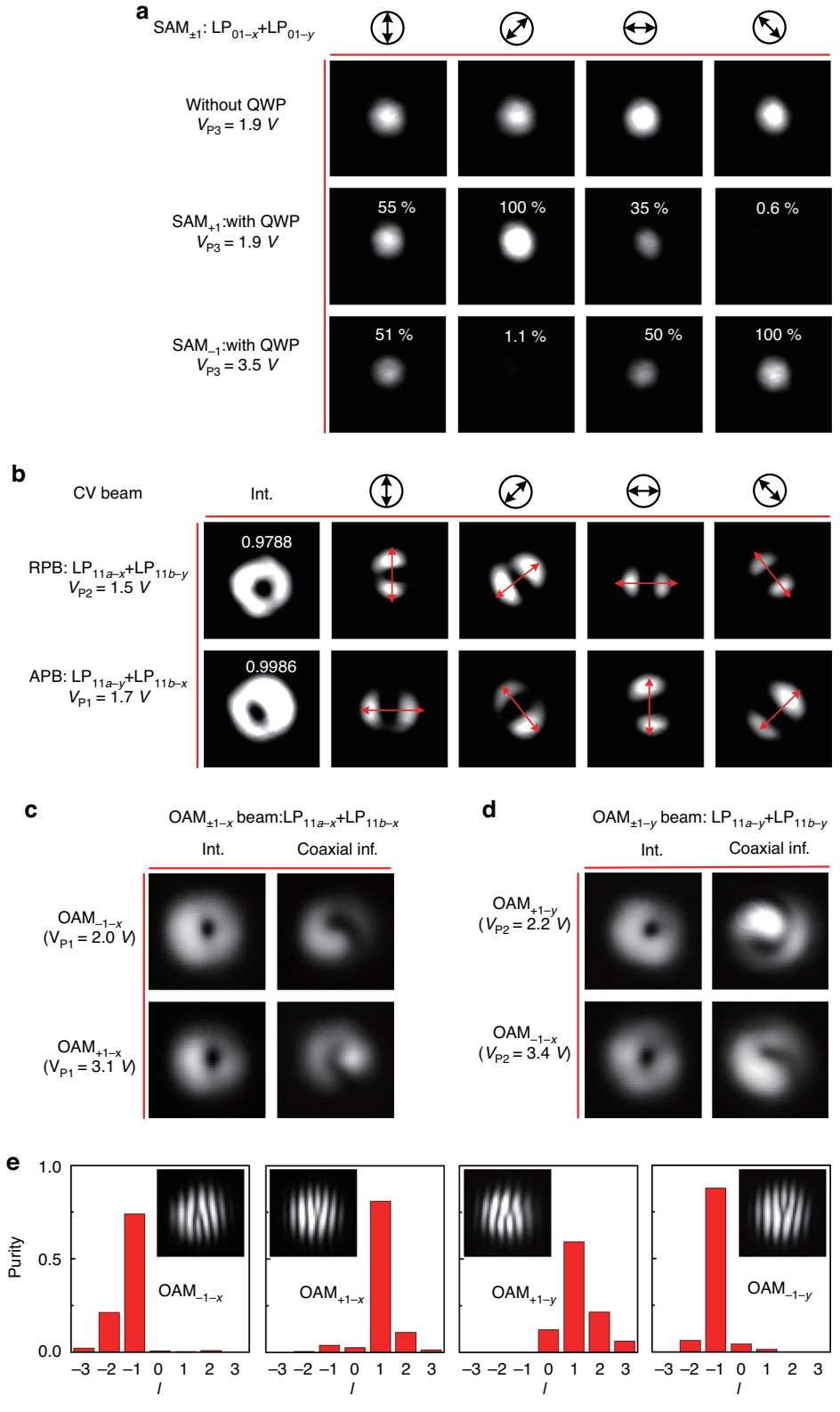

Fig. 4 (See legend on next page.)

Fig. 4 The experimental synthesis of structured light beams. a The $SAM_{\pm1}$ beam is synthesized by incorporating the $LP_{01\text{-}x}$ and $LP_{01\text{-}y}$ modes and characterized with the quarter-wave plate (QWP) rotation method. Top panel: the synthesized structured light ($V_{P3} = 1.9$ V) passes through a polarizer with different orientations (see the black arrows), and the mode intensity remains unchanged; Middle panel: after inserting a QWP behead the polarizer, constructive interference occurs at the 45°-orientated polarizer, and destructive interference occurs at the 135°-orientated polarizer, confirming the structured light carries SAM_{+1}; Bottom panel: when further increasing V_{P3} to 3.5 V, the constructive interference and the destructive interference exchange with each other, confirming the structured light carries SAM_{-1}. **b** The CV beams are synthesized by incorporating the LP_{11a} and LP_{11b} modes with different polarizations. Top panel: the RPB is synthesized with the combination of $LP_{11a\text{-}x}$ and $LP_{11b\text{-}y}$ modes at $V_{P2} = 1.5$ V. It has a donut intensity pattern, and maps to an LP_{11} mode with a mode azimuth (red arrow) same as the orientation of the polarizer; Bottom panel: the APB is synthesized with the combination of $LP_{11a\text{-}y}$ and $LP_{11b\text{-}x}$ modes at $V_{P1} = 1.7$ V, and it also has a donut intensity pattern, but maps to an LP_{11} mode with a mode azimuth angle vertical to the orientation of the polarizer. **c** The $OAM_{\pm1\text{-}x}$ beam is synthesized with the combination of the $LP_{11a\text{-}x}$ and $LP_{11b\text{-}x}$ modes. The intensity, and coaxial interference (inf.), patterns confirm the generation of $OAM_{-1\text{-}x}$ (top panel, at $V_{P1} = 2$ V) and $OAM_{+1\text{-}x}$ (bottom panel, at $V_{P1} = 3.1$ V). **d** The $OAM_{\pm1\text{-}y}$ beam is synthesized with the combination of the $LP_{11a\text{-}y}$ and $LP_{11b\text{-}y}$ modes. The intensity and coaxial interference (inf.) patterns confirm the generation of $OAM_{-1\text{-}x}$ (top panel, at $V_{P2} = 2.2$ V) and $OAM_{+1\text{-}x}$ (bottom panel, at $V_{P2} = 3.4$ V). **e** Modal decomposition into the OAM basis for $OAM_{-1\text{-}x}$, $OAM_{+1\text{-}x}$, $OAM_{+1\text{-}y}$, and $OAM_{-1\text{-}y}$ light beam, respectively. Insets: the corresponding off-axis interference patterns. (@1550 nm)

successfully. By further increasing the applied voltage V_{P1} to 3.1 V thus adjusting the phase difference to -π/2, one can also generate the $OAM_{+1\text{-}x}$ beam, as shown in the bottom panel of Fig. 4c. It can be seen that the generated $OAM_{+1\text{-}x}$ beam has a donut-shaped intensity pattern and an anti-clockwise helical coaxial interference pattern. Similarly, $OAM_{+1\text{-}y}$ and $OAM_{-1\text{-}y}$ beams can also be synthesized with the $LP_{11a\text{-}y}$ and $LP_{11b\text{-}y}$ modes by making the phase difference be -π/2 and π/2 when setting $V_{P2} = 2.2$ and 3.4 V, respectively, as shown in Fig. 4d. To determine the modal purity we perform a modal decomposition into the OAM basis[56], with the results shown in Fig. 4e for $OAM_{-1\text{-}x}$, $OAM_{+1\text{-}x}$, $OAM_{+1\text{-}y}$, and $OAM_{-1\text{-}y}$ light beam, respectively. The insets show the corresponding off-axis interference patterns. We see the majority of the modal power in the desired modal, with small cross-talk contributions from neighboring modes.

Extension to TAM

Theoretically, the proposed all-on-chip structured light generator can synthesize a TAM beam that carries both OAM and SAM. A TAM beam is usually described with a spin-orbit higher-order Poincaré (HOP) multi-sphere as shown in Fig. 5a[37], in which the basis states are more general orthogonal states that incorporate both SAM and OAM[12,57], and the S parameters (S_1, S_2, S_3) are defined as the Stokes parameter of Poincaré sphere[50]. In our case, a TAM beam can be described as follows

$$\mathrm{TAM} = (\cos\theta_1 \cdot \mathrm{O}_x + e^{-i\phi_1} \cdot \sin\theta_1 \cdot \mathrm{O}_y)/\sqrt{2}, \quad (\theta_1 \in [0, 0.5\pi], \phi_1 \in [0, 2\pi]) \tag{2}$$

in which

$$\mathrm{O}_x = (\cos\theta_2 \cdot \mathrm{LP}_{11a-x} + e^{-i\phi_2} \cdot \sin\theta_2 \cdot \mathrm{LP}_{11b-x})/\sqrt{2}, \quad (\theta_2 \in [0, 0.5\pi], \phi_2 \in [0, 2\pi]) \tag{2 − a}$$

$$\mathrm{O}_y = (\cos\theta_3 \cdot \mathrm{LP}_{11a-y} + e^{-i\phi_3} \cdot \sin\theta_3 \cdot \mathrm{LP}_{11b-y})/\sqrt{2}, \quad (\theta_3 \in [0, 0.5\pi], \phi_3 \in [0, 2\pi]) \tag{2 − b}$$

Therefore, a TAM beam can be synthesized with four LP_{11} modes (i.e., $LP_{11a\text{-}x}$, $LP_{11a\text{-}y}$, $LP_{11b\text{-}x}$, $LP_{11b\text{-}y}$) and carries six parameters (i.e., θ_1, φ_1, θ_2, φ_2, θ_3, and φ_3). More details about these parameters are explained below.

(1) θ_2 and ϕ_2 decide the power ratio and phase difference between the $LP_{11a\text{-}x}$ and $LP_{11b\text{-}x}$ modes, determining the phase structure of the E_x component of the TAM beam, as shown in Fig. 5a sphere II.

(2) θ_3 and ϕ_3 decide the power ratio and phase difference between the $LP_{11a\text{-}x}$ and $LP_{11b\text{-}x}$ modes, determining the phase structure of the E_y component of the TAM beam, as shown in Fig. 5a sphere III.

(3) θ_1 and ϕ_1 decide the power ratio and phase difference between the O_x and O_y components, determining the polarization state of the TAM beam, as shown in Fig. 5a sphere I.

As an example, Fig. 5b shows some of the synthesized TAMs, showing their intensity/polarization patterns, and the phase structures of their E_x and E_y components. In these examples, the $\theta_1 = \theta_2 = \theta_3 = \pi/4$, thus all four LP_{11} modes are excited equally. And the phase terms φ_2 and φ_3 are chosen to be π/2 or 3π/2 so that both E_x and E_y components carry $OAM_{\pm1}$; while φ_1 is appropriately chosen to produce the linear polarization (e.g., [θ_1, θ_2, θ_3, φ_1, φ_2, φ_3]=[π/4, π/4, π/4, π/2, π/2, π/2] or =[π/4, π/4, π/4, 3π/2, 3π/2, 3π/2]) or the vortex-like polarization (e.g., [θ_1, θ_2, θ_3, φ_1, φ_2, φ_3]=[π/4, π/4, π/4, 0, π/2, π/2] or =[π/4, π/4, π/4, π/2, 3π/2, π/2]), respectively. For the structured light with [θ_1, θ_2, θ_3, φ_1, φ_2, φ_3]=[π/4, π/4, π/

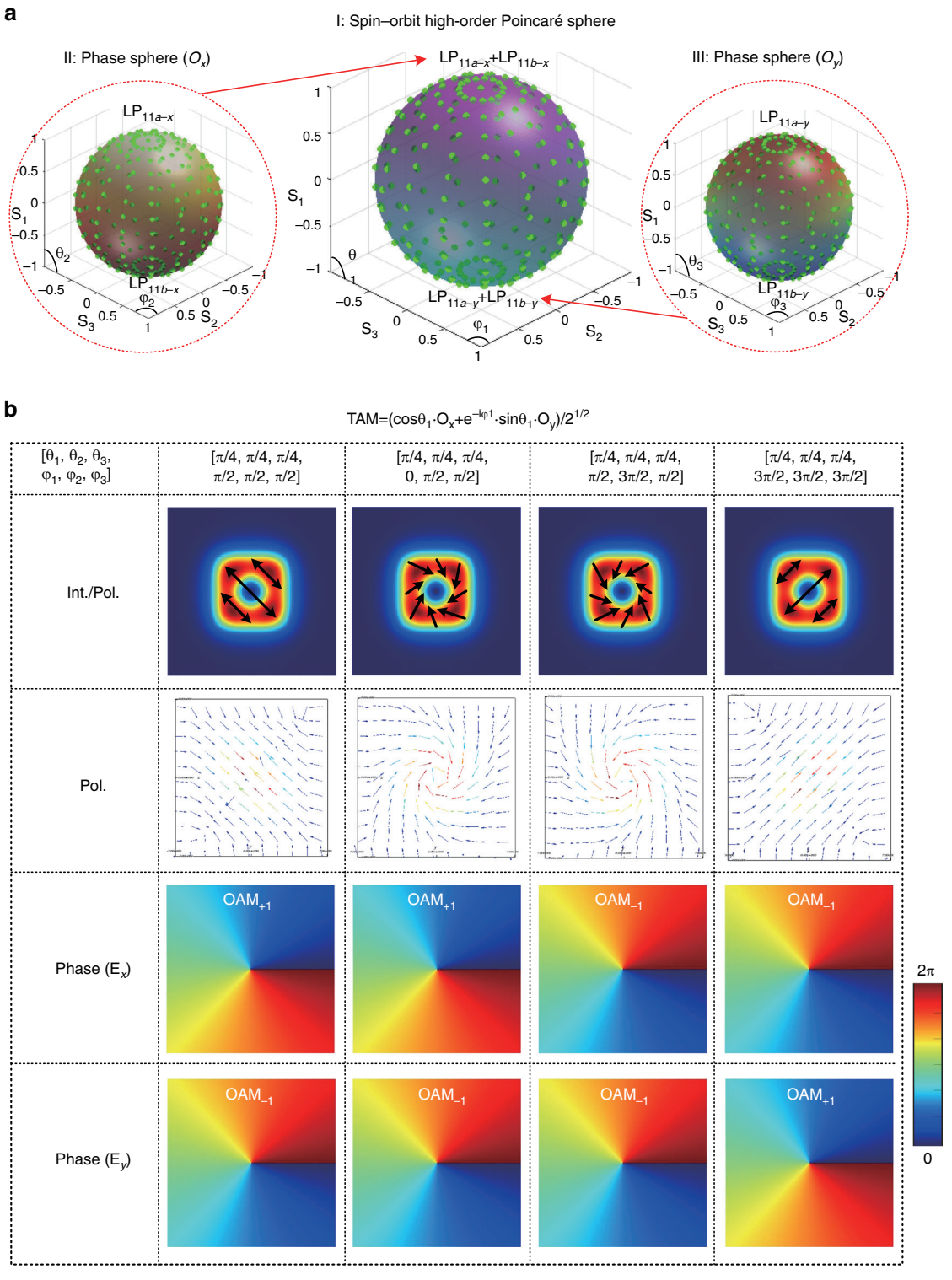

Fig. 5 The synthesis of the TAM beams. a Schematic of the synthesis of the TAM beam by stimulating $LP_{11a\text{-}x}$, $LP_{11a\text{-}y}$, $LP_{11b\text{-}x}$, $LP_{11b\text{-}y}$ modes, spin-orbit high-order Poincaré multi-sphere (I) show the polarization sphere of the TAM beam, while inset (II) and (III) show the phase sphere of the O_x and O_y components of the TAM beam. **b** The intensity/polarization patterns, phase structure of the E_x component, and phase structure of the E_y component of the synthesized typical TAM beam with different phases [θ_1, θ_2, θ_3, φ_1, φ_2, φ_3]. When [θ_1, θ_2, θ_3, φ_1, φ_2, φ_3]=[π/4, π/4, π/4, π/2, π/2, π/2], the structured light has a donut intensity, 135° linear polarization and carries $OAM_{+1\text{-}x}$ and $OAM_{+1\text{-}y}$; When [θ_1, θ_2, θ_3, φ_1, φ_2, φ_3]=[π/4, π/4, π/4, 0, π/2, π/2], the structured light has a donut intensity, clockwise-vortex polarization and carries $OAM_{+1\text{-}x}$ and $OAM_{+1\text{-}y}$; [θ_1, θ_2, θ_3, φ_1, φ_2, φ_3]=[π/4, π/4, π/4, π/2, 3π/2, π/2], the structured light has a donut intensity, anticlockwise-vortex polarization, and carries $OAM_{-1\text{-}x}$ and $OAM_{-1\text{-}y}$; When [θ_1, θ_2, θ_3, φ_1, φ_2, φ_3] =[π/4, π/4, π/4, 3π/2, 3π/2, 3π/2], the structured light has a donut intensity, 45° linear polarization, and carries $OAM_{-1\text{-}x}$ and $OAM_{+1\text{-}y}$

4, 0, π/2, π/2] considered as an example, it has clockwise vortex-like polarization distribution, and the components of E_x and E_y carry OAM_{+1}, OAM_{-1}, respectively. By appropriately choosing the phase differences [θ_1, θ_2, θ_3, φ_1, φ_2, φ_3], one can traverse the entire HOP multisphere and synthesize the desired light beams carrying $OAM_{\pm 1\text{-}x}$, $OAM_{\pm 1\text{-}y}$, and SAM[41], simultaneously. To generate the aforementioned TAM beams, the powers and phases of these four LP_{11} modes should be accuracy adjusted. However, it is difficult to achieve due to the thermal crosstalk. One can adopt the structures of air trenches, free-standing[58] to increase the thermal efficiency and thus decrease mode crosstalk.

Discussion

In summary, we have demonstrated an all-on-chip reconfigurable structured light generator by incorporating an SOI chip with a silica chip. Our work advances the nascent field of PICs for structured light creation, showing how to both create and control the light all on-chip without the clumsy external free-space conversion (which negates the very benefit of starting on-chip in the first place). We demonstrate its power by going beyond the state-of-the-art and showing full angular momentum control, from scalar orbital angular momentum (OAM) to vectorial combinations, made possible by full polarization control. Not only do we create this on-chip, but we also keep it there, with direct control and delivery through a waveguide. Further, our device has a fiber input and fiber output for a truly integrated, compact and reconfigurable solution, showing excellent performance in modal spectrum, wavelength spectrum and speed. We believe that this makes our solution idea for applications such as mode division multiplexing in fiber, fiber sensing with structured light and on-chip quantum technologies based on the spatial modes of light.

The proposed structured light generator can synthesize more complex total angular momentum beams by stimulating four LP_{11} modes simultaneously. While to scale to a higher order OAM state, one should design a silica mode multiplexer supporting higher order LP modes such as LP_{21a}, LP_{21b}, and LP_{20} modes, by using the cascaded vertical coupler[59] or mode rotator based on a trenched waveguide[60]. Moreover, the thermal crosstalk increases as the number of activated phase shifters, which results in the inaccurate power and phase difference of these model basis. To address this issue, structures like air trenches and free-standing[58] can be adopted. These structures can enhance the thermal efficiency of the phase shifter, thereby reducing mode crosstalk.

Compared with the methods reported previously on-chip generating structured light, the scheme proposed here shows a prominent advantage of versatility, broad bandwidth, and high conversion efficiency. Since the silica MBW can be butt-coupled efficiently to an FMF with a low coupling loss of <2 dB or less for all six LP modes by using the proposed multimode segmented waveguide[61], the structured light beams synthesized by the present all-on-chip generator can be guided into an OAM fiber conveniently for remote applications. Regarding mode fidelity characterization, while current experimental limitations prevent comprehensive modal purity analysis across the entire structured light spectrum, we have established a theoretical framework correlating output fidelity with two fundamental parameters: intrinsic mode purity of the LP basis states, and precision in amplitude and phase control of modal superposition. Our experimental measurements confirm intermodal crosstalk suppression below -14.2 dB for all six LP modes[53]. Through rigorous optimization of relative power ratios and phase differences among constituent modes, as demonstrated in our previous work[50], our scheme expects to achieve a high theoretical mode fidelity. For further development, efforts should be concentrated on optimizing and simplifying the chip architecture. This can be achieved by employing the structures of a variable power splitter[62], 2-D grating coupler[63] and high-efficiency phase shifter[58], thus decreasing the insertion loss and thermal crosstalk. Through these means, the insertion loss and thermal crosstalk can be significantly reduced. Once the chip architecture is enhanced, it becomes possible to delve into the generation of more intricate TAM beams and skyrmions, as indicated in reference[64,65]. Additionally, these various structured light beams can be utilized in communication[63,66] and particle manipulation[67].

Methods

Silicon photonic chip design

Figure 6a shows the schematic configuration of the SOI chip that produces three pairs of TE_0/TM_0 modes whose power ratios and phase shifts can be tuned thermally. The SOI chip consists of a PBS, seven 1 × 2 MMI 3-dB couplers, six variable optical attenuators (VOAs; A_1, A_2, …, A_6), six phase shifters (PSs; P_1, P_2, …, P_6), three PSRs (R_1, R_2, R_3), and four ECs (EC_i, EC_1, EC_2, EC_3). Among them, 1 × 2 MMIs, VOAs, phase shifters, and ECs are relatively robust and have a fabrication tolerance of tens of nanometers. However, the PBS and PSR used for polarization manipulation have more critical fabrication requirements. To address this, we have adopted new structures (such as bent directional coupler and adiabatic coupler)[49] and mechanisms (such as mode hybridity)[51] to increase the bandwidth, fabrication tolerance, and polarization extinction ratio of the PBS and PSR. Therefore, the designed silicon chip has good performance and fabrication reproducibility. Figure 6b shows the cross-section of the silicon photonic waveguide, which has a 220-nm-thick silicon core layer surrounded by silica, and a metal micro-

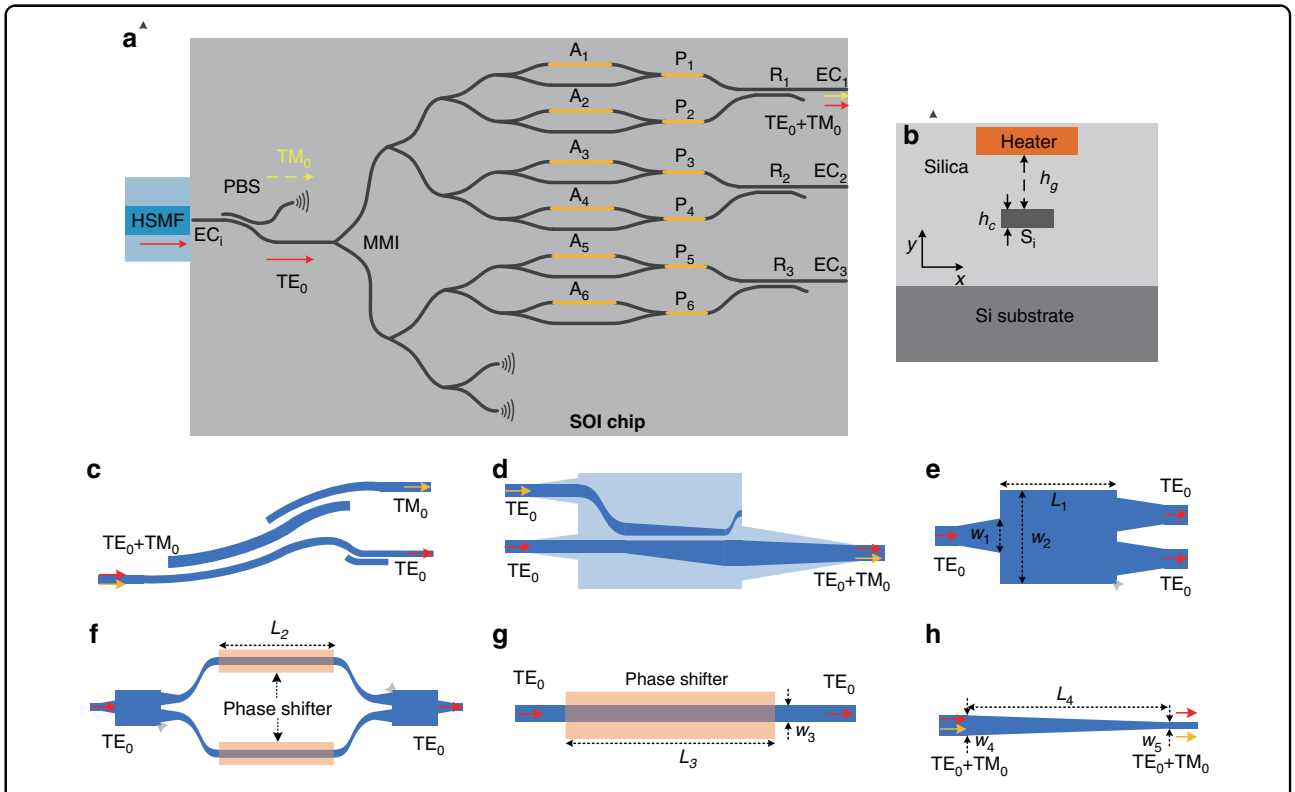

Fig. 6 Silicon photonic chip. a Schematic configuration of the SOI chip, which consists of a polarization beam splitter (PBS), seven 1×2 3-dB multimode interference (MMI) couplers, six variable optical attenuators (VOAs; A_1, A_2, …, A_6), six phase shifters (PSs; P_1, P_2, …, P_6), three polarization-splitter rotators (PSRs; R_1, R_2, R_3), and four edge couplers (EC; EC_1, EC_2, EC_3). **b** The silicon waveguide cross-section. The schematic configuration of the (**c**) PBS, (**d**) PSR, (**e**) 1×2 MMI coupler, (**f**) VOA, (**g**) PS, and (**h**) EC

heater is located on the top with a separation of $h_g = 1.5$ μm to balance the heating efficiency and optical absorption loss. The PBS used here is designed based on the bent directional coupler as shown in Fig. 6c proposed in[49]. The PSR used here works on the principle of mode hybridness of the tapered ridge waveguide, and a directional coupler is further used to separate the TE_0 and TM_0 modes, as shown in Fig. 6d[51,52]. The 1 × 2 3-dB coupler is designed based on MMI as shown in Fig. 6e. The VOAs are designed based on a symmetric 1 × 1 Mach-Zender interferometer (MZI) as shown in Fig. 6f. The designed phase shifters are shown in Fig. 6g, which utilizes the effective thermo-optical coefficient difference between the TE_0 and TM_0 modes in a silicon photonic waveguide, and the waveguide width of 0.45 μm is chosen to balance the thermal efficiency and transmission loss[50]. The EC based on an inverse taper structure at the two ends of the SOI is used for the butt coupling between the SOI chip and HSMF or silica single mode waveguide, as shown in Fig. 6h. The inverse taper is linearly tapered from 0.45 to 0.16 μm, thus well matching the mode field of the HSMF or silica single mode waveguide. The key parameters of the designed silicon components are summarized in Table 2.

Table 2 The key parameters of the designed silicon photonic devices

Parameters	w_1	w_2	w_3	w_4	w_5	L_1	L_2	L_3	L_4
Value (μm)	1.6	4	0.45	0.45	0.16	13.75	50	50	180

Silica mode multiplexer design

The three-channel silica mode multiplexer consists of two cascaded adiabatic directional couplers (ADC #1, ADC #2), a mode rotator and has a total length L = 6000 μm as shown in Fig. 7a[53]. The silica mode multiplexer is polarization-insensitive due to the low birefringence and low index contrast. The inset of Fig. 7a shows the cross-section of the silica waveguide, whose index contrast is about 1.5%. In particular, the silica waveguides are designed with two different heights, i.e., $h_1 = 6.5$ μm and $h_2 = 4$, to realize efficient conversion of the LP_{01} and LP_{11b} modes which have different mode-field symmetry[68]. The core sizes of the single mode input waveguide and multimode output waveguide are 4.0×4.0 μm^2 and 6.5×6.5 μm^2, respectively. At the output port, the silica multimode bus waveguide (MBW) can couple to the FMF

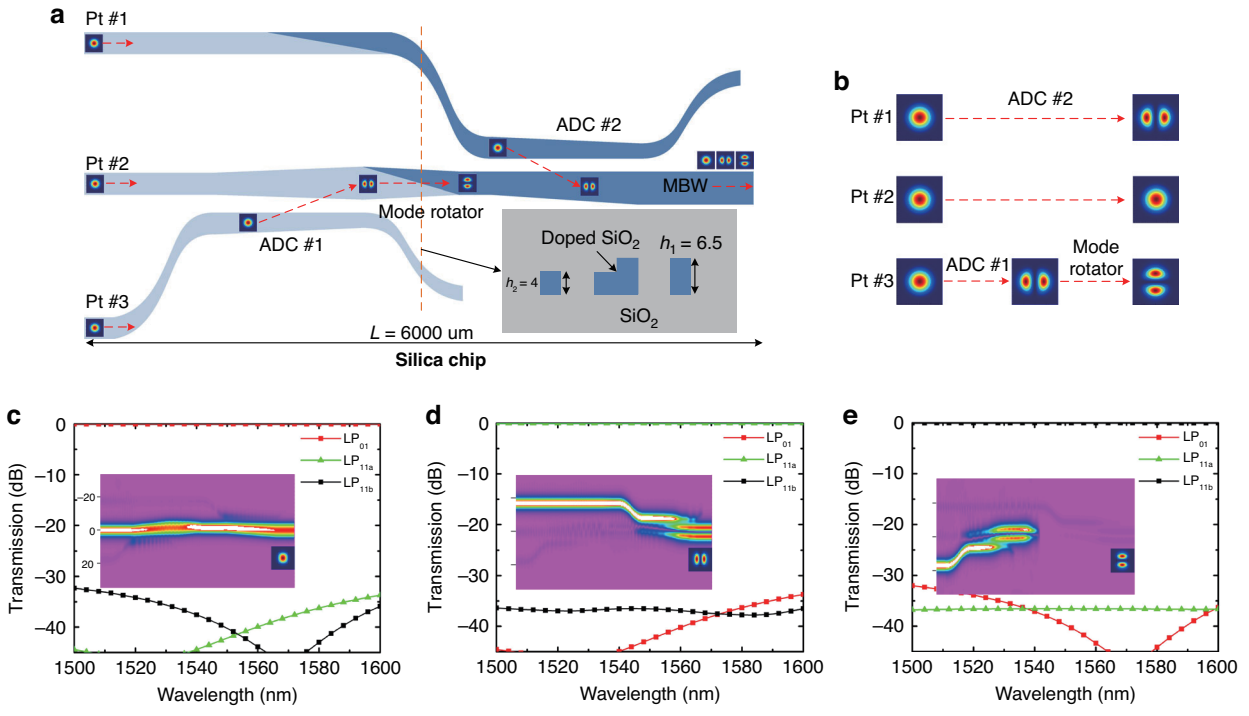

Fig. 7 Silica chip. a Schematic configuration of the silica mode multiplexer, consisting of three input ports (Pt #1, Pt #2, Pt #3), two adiabatic directional couplers (ADC #1 and ADC #2), a mode rotator, and an output silica multimode bus waveguide (MBW). The inset shows the cross-section of the silica waveguide, it has a doped silica core and a pure silica cladding, while the silica single mode waveguide and multimode waveguide are designed with the core heights of $h_2 = 4$ μm and $h_1 = 6.5$ μm, respectively. **b** Operation principle: the LP_{01} mode launched into Pt #1 couples to the LP_{11a} mode of the MBW via ADC #2; the LP_{01} mode launched into Pt #2 passes through the two ADCs directly; the LP_{01} mode launched into Pt #3 is coupled to the LP_{11a} mode of the MBW via ADC #1 first and is then rotated to the LP_{11b} mode with a mode rotator based on the tilt-etched dual-layer waveguide. Simulated transmissions when light launched into **(c)** Pt #2, **(d)** Pt #1, and **(e)** Pt #3, the insets show the corresponding light propagation at 1550 nm

with high efficiency and low crosstalk for the applications. The operation principle of the mode multiplexer is shown with details in Fig. 7b. Here the LP_{01} mode launched into Pt #1 couples to the LP_{11a} mode of the MBW via ADC #2; the LP_{01} mode launched into Pt #2 passes through the two ADCs directly; meanwhile, the LP_{01} mode launched into Pt #3 couples to the LP_{11a} mode of the MBW via ADC #1 first and then rotates to LP_{11b} mode with a mode rotator based on the tilt-etched dual-layer waveguide. The simulated transmissions for the lights launched into Pt #2, Pt #3, and Pt #1 are shown in Fig. 7c–e, respectively, while the insets show the corresponding light propagation for the operation at the wavelength of 1550 nm. The simulation results show the designed mode multiplex has an ultra-low loss less than 0.04 dB and crosstalk less than -32 dB for the LP_{01}, LP_{11a}, and LP_{11b} modes in the wavelength range of 1500-1600 nm. The ultra-low loss and low crosstalk can be attributed to the principle of adiabatic mode evolution in the designed ADCs. The currently proposed structured light beam generator integrates a silicon chip with a silica chip, it is not particularly compact. Future work can consider replacing the silica mode multiplexer with a two-dimensional grating coupler[63] or grating antenna array[66], thus integrating all the modules on one chip.

Acknowledgements
This work is supported by National Natural Science Foundation of China (NSFC) (62375238, 92150302, U23B2047, and 62321166651), Zhejiang Provincial Major Research and Development Program under Grant 2021C01199, The Fundamental Research Funds for the Central Universities, The Leading Innovative and Entrepreneur Team Introduction Program of Zhejiang (2021R01001).

Author details
[1]State Key Laboratory for Extreme Photonics and Instrumentation, College of Optical Science and Engineering, Zhejiang University, Hangzhou 310058, China. [2]State Key Laboratory for Mesoscopic Physics, School of Physics, Peking University, Beijing 100871, China. [3]School of Physics, University of the Witwatersrand, Johannesburg, South Africa

Author contributions
W.K.Z. and D.X.D. conceived the idea. W.K.Z. and X.L.Y. contributed equally to this work. W.K.Z. and R.R.L. designed and fabricated the silicon chip. X.L.Y. designed and fabricated the silica chip. W.K.Z. and X.L.Y. built the setup and carried out the experiment. All authors discussed the results and contributed to the manuscript. W.K.Z., X.L.Y., D.X.D. and A.F. wrote the manuscript. D.X.D. supervised the project.

Data availability
All data are available in the main text or the supplementary materials.

Conflict of interest
Andrew Forbes is an Editor for the journal, and no other author has reported any competing interests.

Supplementary information The online version contains supplementary material available at https://doi.org/10.1038/s41377-025-01899-7.

Received: 4 November 2024 Revised: 2 April 2025 Accepted: 21 May 2025
Published online: 30 June 2025

References

1. Forbes, A., de Oliveira, M. & Dennis, M. R. Structured light. *Nat. Photonics* **15**, 253–262 (2021).
2. Wan, C. H. et al. Toroidal vortices of light. *Nat. Photonics* **16**, 519–522, https://doi.org/10.1038/s41566-022-01013-y (2022).
3. Mao, D. et al. Generation of polarization and phase singular beams in fibers and fiber lasers. *Adv. Photonics* **3**, 014002 (2021).
4. Forbes, A., Ramachandran, S. & Zhan, Q. W. Photonic angular momentum: progress and perspectives. *Nanophotonics* **11**, 625–631 (2022).
5. Sarmiento-Merenguel, J. D. et al. Demonstration of integrated polarization control with a 40 dB range in extinction ratio. *Optica* **2**, 1019–1023 (2015).
6. Lin, Z. J. et al. High-performance polarization management devices based on thin-film lithium niobate. *Light Sci. Appl.* **11**, 93 (2022).
7. Dong, J. L. & Chiang, K. S. Temperature-insensitive mode converters with CO2-laser written long-period fiber gratings. *IEEE Photonics Technol. Lett.* **27**, 1006–1009 (2015).
8. Mao, D. et al. All-fiber radially/azimuthally polarized lasers based on mode coupling of tapered fibers. *Opt. Lett.* **43**, 1590–1593 (2018).
9. Xie, Z. W. et al. Integrated (de)multiplexer for orbital angular momentum fiber communication. *Photonics Res.* **6**, 743–749 (2018).
10. Ni, J. C. et al. Multidimensional phase singularities in nanophotonics. *Science* **374**, eabj0039 (2021).
11. Holleczek, A. et al. Classical and quantum properties of cylindrically polarized states of light. *Opt. Express* **19**, 9714–9736 (2011).
12. Naidoo, D. et al. Controlled generation of higher-order Poincaré sphere beams from a laser. *Nat. Photonics* **10**, 327–332 (2016).
13. Min, C. et al. Focused plasmonic trapping of metallic particles. *Nat. Commun.* **4**, 2891 (2013).
14. Zhang, Y. Q. et al. Plasmonic tweezers: for nanoscale optical trapping and beyond. *Light Sci. Appl.* **10**, 59 (2021).
15. Stilgoe, A. B., Nieminen, T. A. & Rubinsztein-Dunlop, H. Controlled transfer of transverse orbital angular momentum to optically trapped birefringent microparticles. *Nat. Photonics* **16**, 346–351 (2022).
16. Xie, X. S. et al. Harnessing the point-spread function for high-resolution far-field optical microscopy. *Phys. Rev. Lett.* **113**, 263901 (2014).
17. Mao, D. et al. Optical vortex fiber laser based on modulation of transverse modes in two mode fiber. *APL Photonics* **4**, 060801 (2019).
18. Wang, J. et al. Terabit free-space data transmission employing orbital angular momentum multiplexing. *Nat. Photonics* **6**, 488–496 (2012).
19. Wang, J. et al. Orbital angular momentum and beyond in free-space optical communications. *Nanophotonics* **11**, 645–680 (2022).
20. Dholakia, K. & Čižmár, T. Shaping the future of manipulation. *Nat. Photonics* **5**, 335–342 (2011).
21. Paterson, L. et al. Controlled rotation of optically trapped microscopic particles. *Science* **292**, 912–914 (2001).
22. Roy, B. et al. Manifestations of geometric phase and enhanced spin Hall shifts in an optical trap. *N. J. Phys.* **16**, 083037 (2014).
23. Fang, L., Padgett, M. J. & Wang, J. Sharing a common origin between the rotational and linear Doppler effects. *Laser Photonics Rev.* **11**, 1700183 (2017).
24. Liu, J. & Wang, J. Demonstration of polarization-insensitive spatial light modulation using a single polarization-sensitive spatial light modulator. *Sci. Rep.* **5**, 9959 (2015).
25. Maurer, C. et al. What spatial light modulators can do for optical microscopy. *Laser Photonics Rev.* **5**, 81–101 (2011).
26. Liu, T., Chen, S. P. & Hou, J. Selective transverse mode operation of an all-fiber laser with a mode-selective fiber Bragg grating pair. *Opt. Lett.* **41**, 5692–5695 (2016).
27. Zhao, H. et al. All-fiber second-order orbital angular momentum generator based on a single-helix helical fiber grating. *Opt. Lett.* **44**, 5370–5373 (2019).
28. Wong, G. K. L. et al. Excitation of orbital angular momentum resonances in helically twisted photonic crystal fiber. *Science* **337**, 446–449 (2012).
29. Wang, T. et al. High-order mode direct oscillation of few-mode fiber laser for high-quality cylindrical vector beams. *Opt. Express* **26**, 11850–11858 (2018).
30. Chen, R. S. et al. High efficiency all-fiber cylindrical vector beam laser using a long-period fiber grating. *Opt. Lett.* **43**, 755–758 (2018).
31. Fu, S. Y. et al. Orbital angular momentum comb generation from azimuthal binary phases. *Adv. Photonics Nexus* **1**, 016003 (2022).
32. Forbes, A. Structured light from lasers. *Laser Photonics Rev.* **13**, 1900140 (2019).
33. Forbes, A., Mkhumbuza, L. & Feng, L. Orbital angular momentum lasers. *Nat. Rev. Phys.* **6**, 352–364, https://doi.org/10.1038/s42254-024-00715-2 (2024).
34. Carlon Zambon, N. et al. Optically controlling the emission chirality of microlasers. *Nat. Photonics* **13**, 283–288 (2019).
35. Shao, Z. K. et al. On-chip switchable radially and azimuthally polarized vortex beam generation. *Opt. Lett.* **43**, 1263–1266 (2018).
36. Zhang, Z. F. et al. Tunable topological charge vortex microlaser. *Science* **368**, 760–763 (2020).
37. Zhang, Z. F. et al. Spin–orbit microlaser emitting in a four-dimensional Hilbert space. *Nature* **612**, 246–251 (2022).
38. Strain, M. J. et al. Fast electrical switching of orbital angular momentum modes using ultra-compact integrated vortex emitters. *Nat. Commun.* **5**, 4856 (2014).
39. Devlin, R. C. et al. Arbitrary spin-to–orbital angular momentum conversion of light. *Science* **358**, 896–901 (2017).
40. Li, G. X. et al. Spin-enabled plasmonic metasurfaces for manipulating orbital angular momentum of light. *Nano Lett.* **13**, 4148–4151 (2013).
41. Zhou, N. et al. Ultra-compact broadband polarization diversity orbital angular momentum generator with 3.6 × 3.6 μm2 footprint. *Sci. Adv.* **5**, eaau9593 (2019).
42. Zheng, S., Zhao, Z. Y. & Zhang, W. F. Versatile generation and manipulation of phase-structured light beams using on-chip subwavelength holographic surface gratings. *Nanophotonics* **12**, 55–70 (2023).
43. Cai, X. L. et al. Integrated compact optical vortex beam emitters. *Science* **338**, 363–366 (2012).
44. Zhang, C. et al. High efficiency grating coupler for coupling between single-mode fiber and SOI waveguides. *Chin. Phys. Lett.* **30**, 014207 (2013).
45. Raval, M., Poulton, C. V. & Watts, M. R. Unidirectional waveguide grating antennas with uniform emission for optical phased arrays. *Opt. Lett.* **42**, 2563–2566 (2017).
46. Zhong, H. Z. et al. Gigahertz-rate-switchable wavefront shaping through integration of metasurfaces with photonic integrated circuit. *Adv. Photonics* **6**, 016005 (2024).
47. Bütow, J. et al. Generating free-space structured light with programmable integrated photonics. *Nat. Photonics* **18**, 243–249 (2024).
48. Won, R. On-chip ultrafast wavefront shaping. *Nat. Photonics* **18**, 213–213 (2024).
49. Wu, H., Tan, Y. & Dai, D. X. Ultra-broadband high-performance polarizing beam splitter on silicon. *Opt. Express* **25**, 6069–6075 (2017).
50. Zhao, W. K. et al. Ultracompact silicon on-chip polarization controller. *Photonics Res.* **12**, 183–193 (2024).
51. Zhao, W. K. et al. 96-Channel on-chip reconfigurable optical add-drop multiplexer for multidimensional multiplexing systems. *Nanophotonics* **11**, 4299–4313 (2022).
52. Yin, Y. L., Li, Z. Y. & Dai, D. X. Ultra-broadband polarization splitter-rotator based on the mode evolution in a dual-core adiabatic taper. *J. Lightwave Technol.* **35**, 2227–2233 (2017).
53. Yi, X. L. et al. Efficient mode coupling/(de)multiplexing between a few-mode fiber and a silicon photonic chip. *Photonics Res.* **12**, 2784 (2024).
54. Han, C. H. et al. Slow-light silicon modulator with 110-GHz bandwidth. *Sci. Adv.* **9**, eadi5339 (2023).
55. Kharel, P. et al. Breaking voltage–bandwidth limits in integrated lithium niobate modulators using micro-structured electrodes. *Optica* **8**, 357–363 (2021).
56. Ndagano, B. et al. Beam quality measure for vector beams. *Opt. Lett.* **41**, 3407–3410 (2016).
57. Pinnell, J. et al. Modal analysis of structured light with spatial light modulators: a practical tutorial. *J. Optical Soc. Am. A* **37**, C146–C160 (2020).

58. Bomzon, Z., Kleiner, V. & Hasman, E. Pancharatnam–berry phase in space-variant polarization-state manipulations with subwavelength gratings. *Opt. Lett.* **26**, 1424–1426 (2001).
59. Parra, J., Navarro-Arenas, J. & Sanchis, P. Silicon thermo-optic phase shifters: a review of configurations and optimization strategies. *Adv. Photonics Nexus* **3**, 044001 (2024).
60. Huang, Q. D. et al. Mode multiplexer with cascaded vertical asymmetric waveguide directional couplers. *J. Lightwave Technol.* **36**, 2903–2911 (2018).
61. Saitoh, K. et al. PLC-based mode multi/demultiplexers for mode division multiplexing. *Optical Fiber Technol.* **35**, 80–92 (2017).
62. Song, L. J. et al. Toward calibration-free Mach–Zehnder switches for next-generation silicon photonics. *Photonics Res.* **10**, 793–801 (2022).
63. Lu, K. H. et al. Empowering high-dimensional optical fiber communications with integrated photonic processors. *Nat. Commun.* **15**, 3515 (2024).
64. He, T. T. et al. Optical skyrmions from metafibers with subwavelength features. *Nat. Commun.* **15**, 10141 (2024).
65. Lin, W. B. et al. On-chip optical skyrmionic beam generators. *Optica* **11**, 1588–1594 (2024).
66. Milanizadeh, M. et al. Separating arbitrary free-space beams with an integrated photonic processor. *Light Sci. Appl.* **11**, 197 (2022).
67. Wang, B. et al. Topological water-wave structures manipulating particles. *Nature* **638**, 394–400, https://doi.org/10.1038/s41586-024-08384-y (2025).
68. Zhao, W. K., Chen, K. X. & Wu, J. Y. Broadband mode multiplexer formed with non-planar tapered directional couplers. *IEEE Photonics Technol. Lett.* **31**, 169–172 (2019).